Talanta 119 (2014) 156–163

Contents lists available at ScienceDirect

Talanta

journal homepage: www.elsevier.com/locate/talanta

Nickel hydroxide nanoparticles-reduced graphene oxide nanosheets film: Layer-by-layer electrochemical preparation, characterization and rifampicin sensory application

Shokoufeh Rastgar [a], Saeed Shahrokhian [a,b,*]

[a] Department of Chemistry, Sharif University of Technology, Tehran 11155-9516, Iran
[b] Institute for Nanoscience and Technology, Sharif University of Technology, Tehran, Iran

ARTICLE INFO

Article history:
Received 26 August 2013
Received in revised form
18 October 2013
Accepted 22 October 2013
Available online 7 November 2013

Keywords:
Graphene oxide
Reduced graphene oxide
Nickel hydroxide nanoparticles
Rifampicin

ABSTRACT

Electrochemical deposition, as a well-controlled synthesis procedure, has been used for subsequently layer-by-layer preparation of nickel hydroxide nanoparticle-reduced graphene oxide nanosheets (Ni$(OH)_2$–RGO) on a graphene oxide (GO) film pre-cast on a glassy carbon electrode surface. The surface morphology and nature of the nano-hybrid film (Ni$(OH)_2$–RGO) was thoroughly characterized by scanning electron and atomic force microscopy, spectroscopy and electrochemical techniques. The modified electrode appeared as an effective electro-catalytic model for analysis of rifampicin (RIF) by using linear sweep voltammetry (LSV). The prepared modified electrode exhibited a distinctly higher activity for electro-oxidation of RIF than either GO, RGO nanosheets or Ni$(OH)_2$ nanoparticles. Enhancement of peak currents is ascribed to the fast heterogeneous electron transfer kinetics that arise from the synergistic coupling between the excellent properties of RGO nanosheets (such as high density of edge plane sites, subtle electronic characteristics and attractive π–π interaction) and unique properties of metal nanoparticles. Under the optimized analysis conditions, the modified electrode showed two oxidation processes for rifampicin at potentials about 0.08 V (peak I) and 0.69 V (peak II) in buffer solution of pH 7.0 with a wide linear dynamic range of 0.006–10.0 μmol L^{-1} and 0.04–10 μmol L^{-1} with a detection limit of 4.16 nmol L^{-1} and 2.34 nmol L^{-1} considering peaks I and II as an analytical signal, respectively. The results proved the efficacy of the fabricated modified electrode for simple, low cost and highly sensitive medicine sensor well suited for the accurate determinations of trace amounts of rifampicin in the pharmaceutical and clinical preparations.

1. Introduction

It is very important to develop simple, sensitive and accurate methods for detecting active ingredients, since drug monitoring plays an important role in drug quality control and this has a great impact on public health. Besides, development of sensing systems is the main application of nanomaterials, since they can enhance the analytical performance of such devices [1]. Graphene, the basic of carbon-based nanomaterials, is a one-atom-thick planar sheet of sp^2 bonded carbon atoms densely arranged into a 2D honeycomb crystal lattice [2–4]. Thanks to a high specific surface area (theoretically 2630 m^2/g for single-layer graphene) [5], large amounts of edge-planes/defects [6], a high electron transfer rate (15,000 $cm^2/V\,s$) [7], strong mechanical strength and both excellent thermal and electrical conductivities [8], graphene sheets are also ideal materials for electrochemical sensing and biosensing [9,10]. Graphene oxide (GO), a precursor for graphene synthesis, consists of a hexagonal ring-based carbon network having both (largely) sp^2-hybridized carbon atoms and (partly) sp^3-hybridized carbons, which bear oxygen functional groups in the form of hydroxyl and epoxy moieties on the basal plane, with smaller amounts of carboxyl, carbonyl, phenol, lactone and quinone at the sheet edges. These can be viewed as oxidized regions disrupting the extended sp^2 conjugated network of the original honeycomb-lattice structured graphene sheet [11]. Reduced graphene oxide (RGO), product of partially reduction of GO, comprises of nanometer-sized 'islands' of sp^2 graphene separated by invariably residual oxygen-functionalized groups and sp^3 bonding remaining (oxygen fraction around or below 10%), and other defects and vacancies are introduced during reduction [12]. Partial electrochemical reduction of GO provides this importunate for the electrochemist to control the optimal balance between the levels of reduction that can give a reasonable number of functional

* Corresponding author at: Department of Chemistry, Sharif University of Technology, Tehran 11155-9516, Iran. Tel.: +98 21 66005718; fax: +98 21 66002983.
E-mail address: shahrokhian@sharif.edu (S. Shahrokhian).

0039-9140/$ - see front matter © 2013 Elsevier B.V. All rights reserved.
http://dx.doi.org/10.1016/j.talanta.2013.10.047

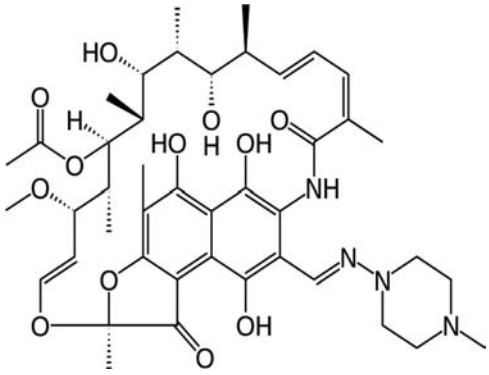

Scheme 1. Chemical structure of rifampicin (RIF).

oxygen groups and defects for electron-transfer reaction while maintaining an appropriately high level of conductivity in the RGO [13,14].

Direct electrochemical deposition of inorganic crystals especially metal nanoparticles, on highly conductive graphene-based substrates, is an attractive approach for thin film based applications, which rising nanocomposites with larger active surface areas and improved electron transport, as an ideal material for the fabrication of electrochemical sensors [14,15]. In this area, various experimental parameters including salt solution concentration, potential and time of deposition can be manipulated to control the nucleation and growth rate of the metal NPs [16].

Rifampicin (RIF), 3-[(4-methyl-1-piperazinyl) imino] methyl rifamycin (Scheme 1) belongs to the class of macrocyclic antibiotics, which contains a naphthohydroquinone ring spanned by a highly substituted aliphatic bridge, and differ from one another in the type and location of the substituent on their aromatic ring. RIF is the most important antibiotic of groups widely used in the treatment of tuberculosis, Hansen's disease (HD) and other serious infections such as HIV, which inhibits bacterial DNA-dependent RNA polymerase. Drug-monitoring in patients during antituberculosis therapy is important, especially in AIDS patients, owing to a global increase in the prevalence of drug-resistant tuberculosis [17–19].

Due to its important role in numerous pathological processes, several analytical methods have been reported in the literature for the rifampicin detection [20–22]. Among these, electrochemical methods have attracted great interest because of their simplicity, rapidness and high sensitivity in detecting RIF without requiring tedious pretreatments [17–19,23–27].

In the present work, we develop a simple and versatile in situ approach for the fabrication of a nano-structured thin film (as a modifier) on the surface of a glassy carbon electrode (GCE) by coating it with a thin layer of GO and then partial electroreduction to RGO by applying constant potential, following it with electro-deposition of $Ni(OH)_2$ nanoparticles, which is capable of forming a uniform and stable thin film on the surface of the electrode. The properties of the $Ni(OH)_2$–RGO thin film electrode were characterized by scanning electron microscopy (SEM), atomic force microscopy (AFM), energy dispersive X-ray spectroscopy (EDS), X-ray photoelectron spectroscopy (XPS), electrochemical impedance spectroscopy (EIS) and cyclic voltammetry (CV) methods. The resulting electrochemical sensor under the optimum conditions (electro-deposition and other experimental parameters) is conveniently applied to determination of RIF with a nanomolar detection limit. Excellent features, like a low detection limit, wide linear dynamic range and high sensitivity of the modified electrode proved the successful application of this sensor for the voltammetric determination of RIF in pharmaceutical preparations and human blood serum samples.

2. Experimental

2.1. Chemicals and reagents

Graphene oxide (GO) was ordered from Graphene Supermarket (Graphene Laboratories, Inc. USA). Rifampicin (RIF) was taken kindly from Excir Daru pharmaceutical company (Tehran, Iran). All other chemicals were of analytical reagent grade from Merck. All aqueous solutions were prepared with doubly distilled deionized water. Stock solutions of RIF were freshly prepared as required in N-dimethylformamide (DMF) solution. The working solutions were prepared by diluting the stock solution with phosphate or acetate buffer solutions. In these experiments, 0.1 mol L^{-1} acetate was used for preparation of pHs 4.0 and 5.0, and 0.1 mol L^{-1} phosphate buffer solution (PBS) for pHs 3.0, 6.0, 7.0 and 8.0. Tablets of RIF (300 mg per tablet) were purchased from local pharmacies. Fresh frozen human blood serum was obtained from Iranian Blood Transfusion Organization. A 2% (v/v) of pure methanol was added to the serum sample. After vortexing each of the samples for 2 min, the precipitated proteins were separated by centrifugation for 10 min at 10,000 rpm. Then, this sample was diluted 10-fold and spiked with the different amounts of standard RIF without extraction for further treatments and applied for the recovery tests in the spiked samples. Each sample was run in triplicate and relative standard deviation (RSD) for each sample was calculated.

2.2. Apparatus

Electro-deposition of reduced graphene oxide (RGO) and $Ni(OH)_2$ nanoparticles on RGO and also voltammetric experiments were performed using a Metrohm potentiostat/galvanostat model 797 VA. A conventional three-electrode system was used with a GC working electrode (unmodified or modified), a saturated Ag/AgCl reference electrode and a Pt wire counter electrode. A digital pH/mV/ion meter (CyberScan model 2500) was used for preparation of the buffer solutions. Scanning electron microscopy (SEM) images were obtained with a VEGA\\TESCAN scanning electron microscopy equipped with energy dispersive X-ray spectroscopy (EDS, RONTEC, QUANTAX). Atomic force microscopy (AFM) experiments were carried out in ambient condition using Veeco CP Research instrument using Si cantilever. X-ray photoelectron spectra (XPS) recorded with an Mg or Al X-ray source at the energies of 1486.6 eV or 1253.6 eV, respectively. Electrochemical impedance spectroscopy (EIS) measurements were performed with a Potentiostat/Galvanostat EG&G model 273 A (Princeton Applied Research, USA) equipped with a Frequency Response Detector model 1025 (Power Suite software), which was used with a frequency between 100 MHz and 10 kHz and a 5 mV rms sinusoidal modulation in 0.1 mol L^{-1} KCl solution containing 1 mmol L^{-1} of both $K_4Fe(CN)_6$ and $K_3Fe(CN)_6$ (1:1 mixture) at the $E_{1/2}$ of the $[Fe(CN)_6]^{3-/4-}$ (0.13 V vs. Ag/AgCl). Voltammetric experiments were carried out in buffered solutions of RIF drug that were deoxygenated by purging with pure nitrogen (99.999% from Roham Gas Company). Nitrogen gas was also flowed over the surface of the test solutions during the experiments.

2.3. Electrochemical preparation of modified electrode

The stable GO aqueous solution was achieved by dispersion of 2.0 mg portion of the GO in 2.0 mL H_2O and homogenized ultrasonically for 5 min. Compared to other insoluble carbon nanostructures like RGO and carbon nanotubes, the negative electrostatic repulsion from ionized carboxylic and phenolic groups of GO made it much easier in applying for electrode coating and modification. Before the modification, the GCE was polished with 0.1 mm alumina slurry on a polishing cloth, rinsed thoroughly with water, sonicated

in water for 5 min and finally dried in air. Two microliter of the prepared GO suspension (1 mg mL^{-1}) was drop coated on the GC electrode surface and dried under ambient conditions. In the deposition step, by applying a constant potential of −1.2 V (vs. Ag/AgCl) for 200 s in N_2-purged 0.1 mol L^{-1} acetate buffer solution of pH 5.0, then rinsed with water and dried at room temperature, a stable electrochemical reduced graphene oxide film can be formed on the surface of GC electrode and the resulted electrode was denoted as RGO/GCE. The in-situ synthesis of nickel hydroxide on the surface of the RGO/GC electrode was carried out by cathodic reduction of a stirred and degassed 1 mmol L^{-1} nickel nitrate in a acetate buffer solution (pH 5.0) by applying a constant potential of −1.0 V (vs. Ag/AgCl) for 100 s. The modification procedure was followed by immersing the modified electrode into 0.1 mol L^{-1} NaOH solution and overlaying of cyclic voltammograms were carried out in the range of −0.50 to 0.80 V (10 scans) at a scan rate of 100 mV s^{-1} (data not shown) for the electro-dissolution and passivation of the nickel oxide layer and the growth of nickel hydroxide film resulting $Ni(OH)_2$–RGO/GCE [28–30]. Before the voltammetric measurements, the modified electrode was cycled five times between 0 and 1 V (scan rate 0.1 V s^{-1}) in a phosphate buffer solution (PBS) of pH 7.0 to obtain a reproducible response. When it was necessary, renewal of the electrode surface was easily accomplished by soaking the modified electrode in PBS and cycling the potential as mentioned above. The modified electrode was prepared daily.

3. Results and discussion

3.1. Characterization of the modified electrode

3.1.1. Morphological properties

The SEM image in Fig. 1(a) clearly indicates flake-like shapes and "wrinkled" surface morphology for the electro-reduced graphene oxide nanosheets. Moreover, the layered RGO sheets were tightly packed with the edges of each individual layer distinguishable from the crumpled areas. This lamellar structure of RGO sheets provides a high rough surface area on the electrode as scaffold for further modification. Followed by electro-reduction of nickel ions, a large number of isolated $Ni(OH)_2$ nanoparticles (with an average diameter of 25 nm) were distributed uniformly on the RGO surface as can be seen in Fig. 1(b) and (c). These Highly dispersed $Ni(OH)_2$NPs on the RGO/GCE support, which resulted in a larger surface area, would be beneficial to improve the sensory application of this modified electrode. To provide topographical information, AFM analysis was performed to establish the surface roughness of the deposited films (Fig. 2). The $Ni(OH)_2$NPs–GO exhibits a smoother surface (root mean square (rms) roughness = 10.86 nm) than that of the RGO film (rms roughness=7.34 nm), which that has a smoother surface than GO (rms roughness= 4.75 nm) (Fig. S1), indicating that RGO acted as a blanket, covering the $Ni(OH)_2$ nanoparticles to increase the extent of surface roughness, and then result in the increase of surface active sites.

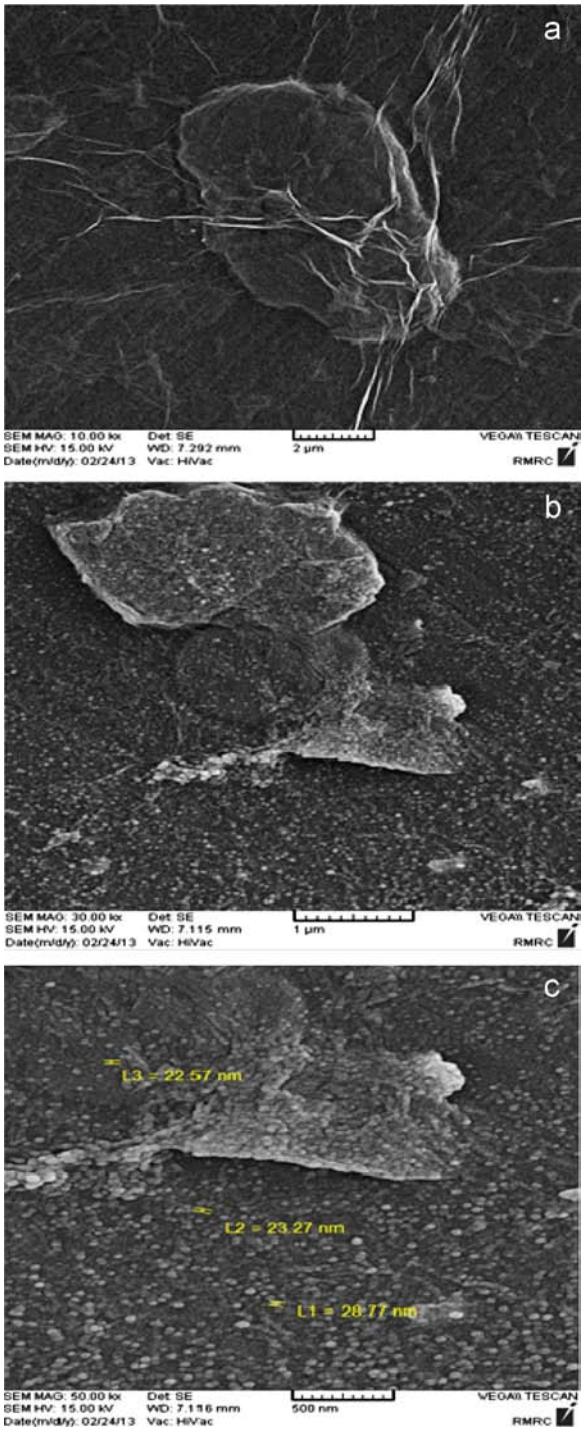

Fig. 1. SEM images (a) RGO, (b) and (c) $Ni(OH)_2$NPs–RGO modified GCE with different resolutions.

3.1.2. Structural properties

Compositions of the GO, RGO and $Ni(OH)_2$–RGO were analyzed via EDS. The EDS spectra of GO and RGO (Fig. 3(a) and (b)) show the main peaks corresponding to C and O elements. The atomic and weight C/O ratio for GO and RGO can be compared quantitatively, which obviously confirmed the decrease of oxygen content in the prepared RGO relative to its precursor material, GO, further characterized the formation of reduced graphene oxide (Tables in inset of Fig. 3(a) and (b)). Additionally, three peaks corresponding to the nickel were clearly observed in the EDS spectrum of $Ni(OH)_2$–RGO at approximately 0.88, 7.5 and 8.2 KeV (Fig. 3(c)), confirming the existence of nickel onto the surface of RGO nanosheets [31,32]. XPS analysis was also performed to characterize the chemical identity of modified electrodes (Fig. S2). The results show that the peaks of oxygen functionalities sharply decreased in RGO structure after the reduction process. A main XPS peak at 858.27 eV is observed for Ni $^2p_{3/2}$, can be assigned to Ni^{+2} in $Ni(OH)_2$ [29]. Hence, under the employed experimental conditions, $Ni(OH)_2$ is formed predominantly during the deposition on the electrode surface.

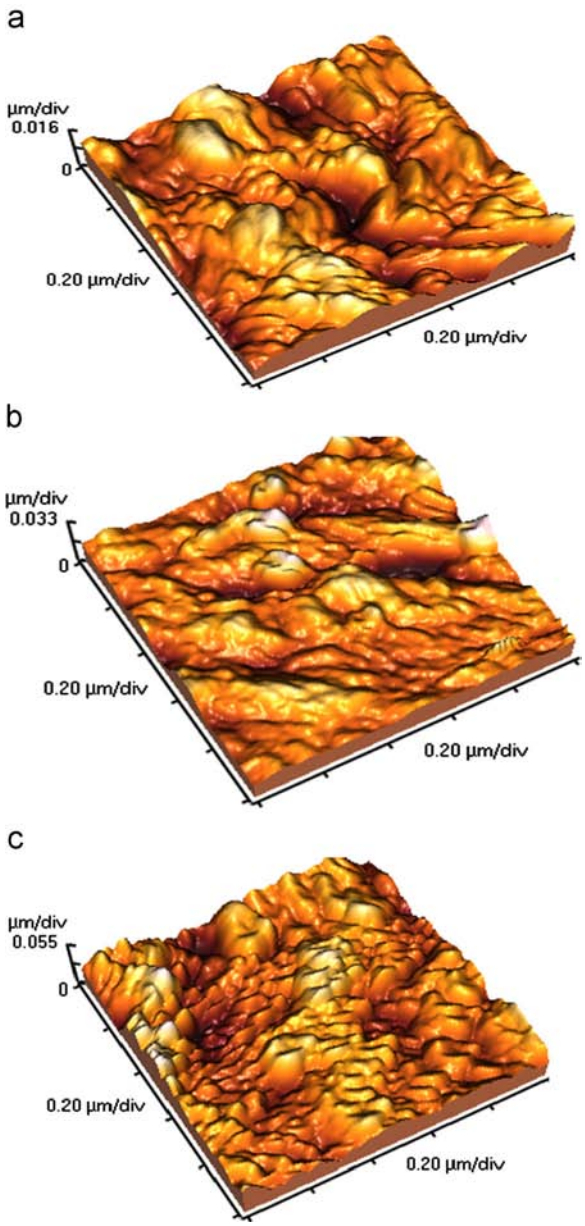

Fig. 2. AFM images of (a) GO, (b) RGO and (c) $Ni(OH)_2$–RGO modified glassy carbon electrodes.

3.1.3. Electrochemical properties

EIS can be used to monitor the interfacial electron transfer resistance at the modified electrodes using a ferro/ferricyanide electrochemical probe. As we can see in Fig. 4(a), when GO is casted onto the GCE surface, the semicircle dramatically increases as compared to the bare GCE, suggesting GO acts as an insulating layer, which increases the interfacial charge transfer resistance. Furthermore, surface charges of the GO repel the access of ferricyanide and ferrocyanide ions to the electrode surface. Using RGO produced electrochemically on the surface of GC, the semicircle vanishes completely. This is mainly ascribed to the improved electrical conductivity of RGO thin films compared to bare GC and GO/GC, probably owing to the restoration of a graphitic network of sp^2 bonds in the produced RGO.

Following the characterization, the electrochemical properties of GO, RGO and $Ni(OH)_2$–RGO were also investigated *via* cyclic voltammetry. To verify the reduction of oxygen containing groups, electrochemical reduction was performed in a nitrogen-purged solution of 0.1 mol L^{-1} PBS (pH=7.0) for GO/GC and RGO/GC as shown in Fig. 4(b). The presence of oxygen functionalities (mainly epoxides, carbonyls, and peroxides) in the GO structure can be confirmed by an intense reduction peak (I_c) appearing at potential lower than −1.10 V, which is attributed to the irreversible reduction of oxygen containing groups [33–36]. The anodic peak (II_a) and cathodic peak (II_c) is ascribed to the redox pair of some electro-active oxygen-containing groups on graphene planes that are too stable to be electrochemically reduced7. In the second cycle (data not shown), the reduction peak current (I_c) at negative potentials decreases considerably and disappears after several potential cycles. This demonstrates that of surface-oxygenated species at GO undergoes a quick and irreversible reduction process and therefore, GO could be reduced electrochemically at negative potentials [34]. In the case of RGO/GCE, the reduction peak (I_c) vanishes completely and a larger redox peak (II_a/II_c) is produced, which corresponded to the residual quinone-type functional groups on the RGO surface, as reported previously [37,38] and also confirmed the successful reduction of GO to RGO.

The formation of the electro-deposited $Ni(OH)_2$ layer on the RGO/GCE surface was also investigated by recording cyclic voltammograms of the modified electrode in 0.1 mol L^{-1} NaOH solution at a scan rate of 100 mV s^{-1} (inset of Fig. 4(b)). An anodic peak is observed at 0.50 V due to the oxidation of the $Ni(OH)_2$ phase to NiO(OH) and in the cathodic (reverse) scan, the NiO(OH) is reduced back to $Ni(OH)_2$ causing a reduction peak at 0.35 V [28–30].

3.1.4. Electrochemical behavior of various electrodes in RIF oxidation

Fig. 5(a) illustrates cyclic voltammetric responses of 10 μmol L^{-1} on the surface of different electrodes. RIF exhibits two very weak oxidation peaks at potentials about 0.2 V (I_a=0.62 μA) and 0.78 V (II_a=0.75 μA) on the bare GCE due to sluggish electron transfer, while the response is considerably improved at the $Ni(OH)_2$/GCE (inset of Fig. 5(a)). In comparison to the bare GCE, a reduction in the overpotential (with $E_p(I_a)$=0.08 V and $E_p(II_a)$=0.69 V) together with a remarkable enhancement in the peak currents by a factor of 2 (I_a=1.25 μA) and 5.32 (II_a=4.2 μA) was observed for RIF in the presence of $Ni(OH)_2$-NPs, indicating the catalytic role of the nickel nanoparticles in the electro-oxidation of RIF. GO/GCE exhibited poor peak currents (with I_a=0.55 μA and II_a=0.5 μA) (inset of Fig. 5(a)) due to the poor conductivity. The peak currents of RIF on the surface of RGO/GCE and $Ni(OH)_2$–RGO/GCE are enhanced, respectively, by a factor of 11.03, 20.00 for peak current (I_a), and 17.00 and 27.00 for peak current (II_a) compared to the bare GCE. In fact, $Ni(OH)_2$-NPs immobilized on the bare GC and RGO/GC surfaces with their large surface area increase the adsorptive sites, resulting in a significant increase in the oxidation peak current. On the other hand, in the presence of RGO nanosheets for the modified electrodes, the electrochemical responses toward RIF are enhanced, resulting from the high density of edge plane-like defective sites and oxygen-containing functionalized group (depend on the reduction extent) on RGO providing more active sites that are beneficial for accelerating electron transfer between the electrode and RIF species in solution. Additionally, π–π stacking interactions between RIF and rich conjugated-structure of graphene resulting in capability to strongly adsorb target species enhance the surface concentration and improve the sensitivity of RIF determination.

3.2. Sensory applications of the modified electrode

3.2.1. Optimization of the experimental parameters

The voltammetric investigations were performed in the pH range of 3.0–8.0 using 0.1 M buffer solutions as supporting electrolyte, containing 10 μmol L^{-1} RIF (Fig. 5(b)). The anodic peaks potentials, shift negatively with pH rising and obtain the slope values of 0.051 V

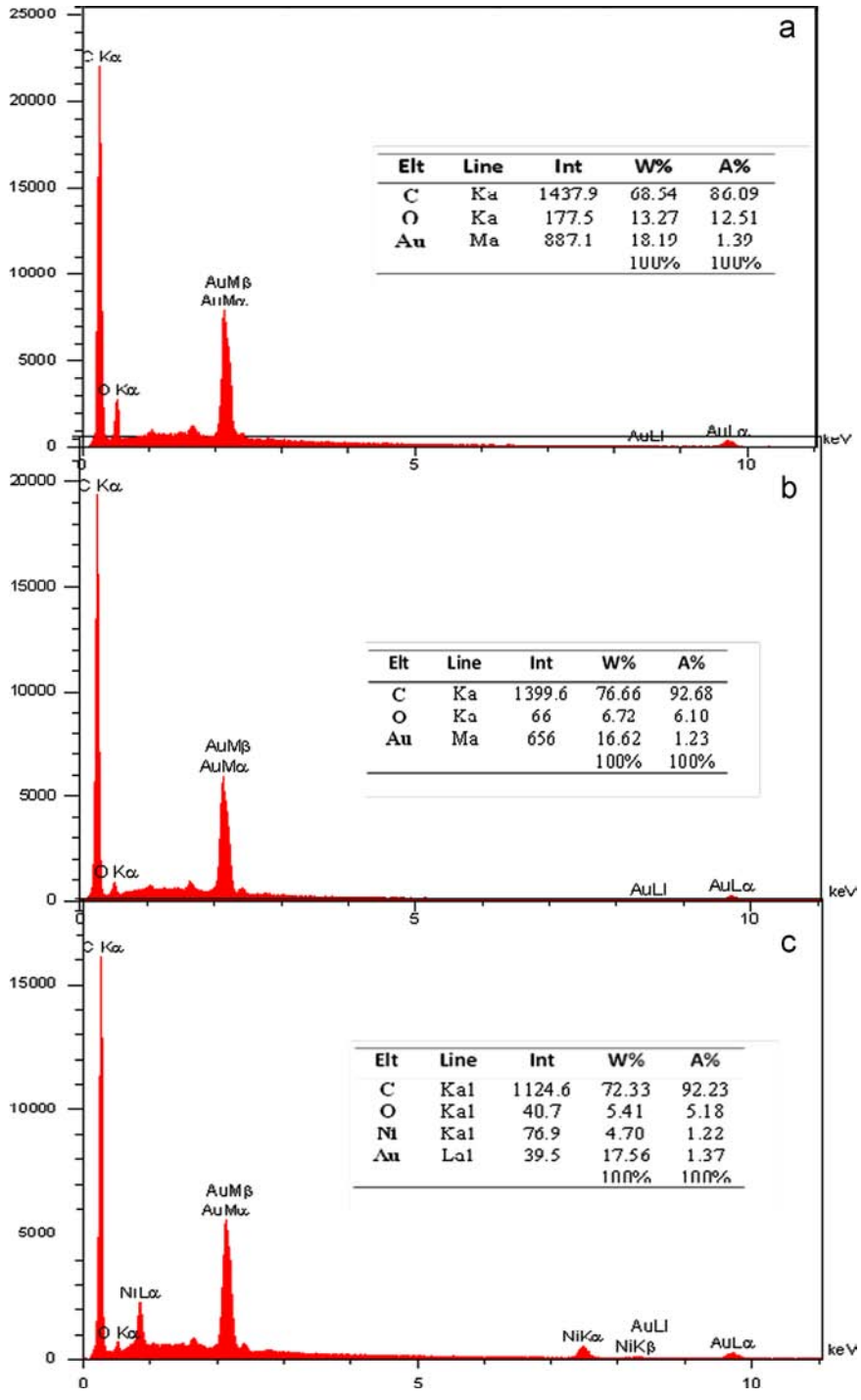

Fig. 3. The EDS pattern of (a) GO/GCE, (b) RGO/GCE and (c) $Ni(OH)_2$–RGO/GCE.

and 0.049 V per pH unit for peaks I and II, respectively, indicating participation of equal numbers of electrons and protons are involved in the electro-oxidation of RIF [39]. By using the anodic current of either peak I or peak II as analytical signals, the maximum peak current found at phosphate buffer solution of pH 7.0 and therefore, that was selected as the supporting electrolyte to obtaining the best sensitivity in all voltammetric determinations (Fig. S3).

LSVs of the buffered solutions (0.1 mol L^{-1}, pH 7.0) containing 10 μmol L^{-1} RIF recorded at different potential sweep rates (10–500 mV s^{-1}). The slope values of 0.66 and 0.62 for the linear variation of the logarithm of the peak currents I and II, respectively, to the logarithm of the sweep rate describe the adsorption of RIF at the modified electrode surface and their diffusion through the nano-porous $Ni(OH)_2$–RGO film [40]. Such behavior has been previously reported as a model of the inter-layer diffusion regime through the porous layer of the CNT on the electrode surface [41,42]. Also, increasing the potential scan rate results in a positive shift of the oxidation peak potentials; this linearly depends on log υ (Fig. S4). According to Laviron's theory [43] and using the slope of $E(V)$ vs. log (V s^{-1}), the number of electrons (n) transferred in the electro-oxidation of RIF was calculated to be 2 and 1 for peaks I and II, respectively.

In the light of the above-mentioned results and also previous works, the electrochemical oxidation of RIF at the $Ni(OH)_2$–RGO/GCE

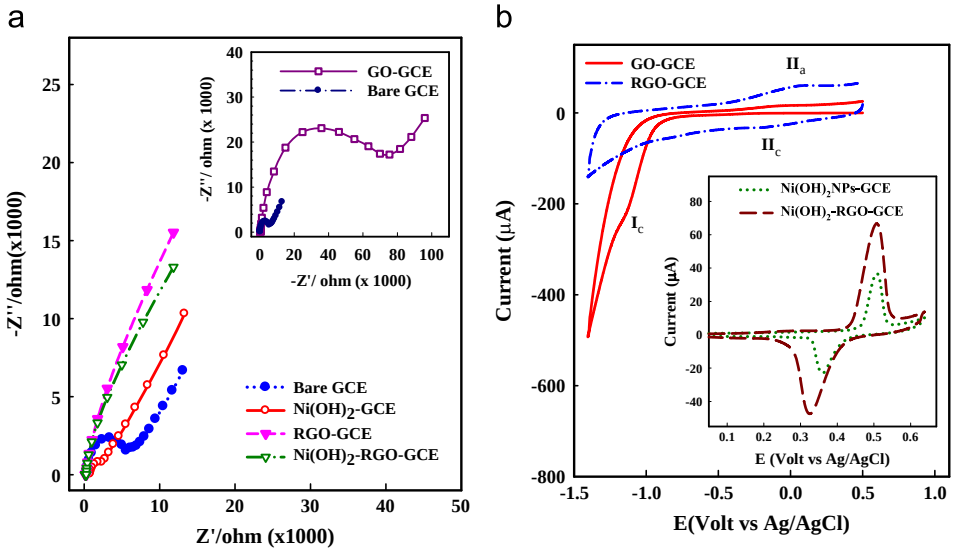

Fig. 4. (a) Nyquist diagram ($-Z''$ vs. Z') for the EIS measurements in 1 mmol L^{-1} $K_3Fe(CN)_6/K_4Fe(CN)_6$ and 0.1 mol L^{-1} KCl at $E_{1/2}=0.13$ V for a bare GCE (•), $Ni(OH)_2$–GO(○), RGO–GCE (▾) and $Ni(OH)_2$–RGO–GCE (▿); inset: GO–GCE (□) and bare GC (•) for comparison. (b) CVs of GO/GCE (solid line, red), RGO–GCE (dashed-dotted line, blue) in 0.1 mol L^{-1} phosphate buffer solution (pH 7.0); inset: CVs of $Ni(OH)_2$–GCE (dotted line, green) and $Ni(OH)_2$–RGO–GCE (dashed line, brown) in the solution of 0.1 mol L^{-1} NaOH. (For interpretation of the references to color in this figure legend, the reader is referred to the web version of this article.)

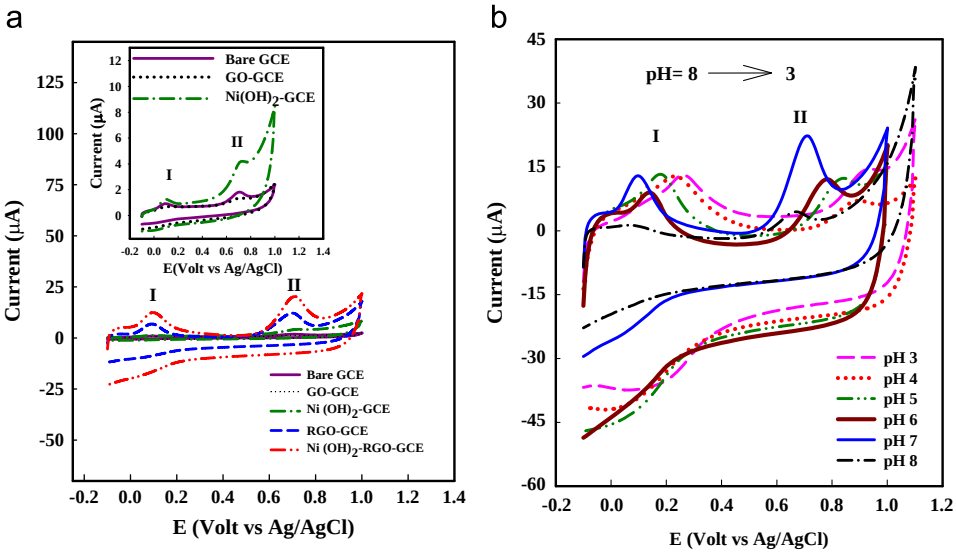

Fig. 5. (a) CVs of 10 μmol L^{-1} of RIF on the surface of various electrodes: bare GCE (solid line, purple), $Ni(OH)_2$–GCE(dashed-dotted line, green), GO–GCE (dotted line, black), RGO–GCE (dashed line, blue) and $Ni(OH)_2$–RGO–GCE (dashed-dotted-dotted line, red). Potential sweep rate was 100 mV s^{-1} and supporting electrolyte was 0.1 mol L^{-1} phosphate buffer solution (pH 7.0). (b) CVs of 10 μmol L^{-1} RIF at the $Ni(OH)_2$–RGO–GCE in various pHs (from 3 to 8) of 0.1 mol L^{-1} PBS. (For interpretation of the references to color in this figure legend, the reader is referred to the web version of this article.)

should be a two-electron and two-proton process for the peak I, which is associated to the oxidation of 6,9-dihydroxynaphthalene moiety to the corresponding naphthoquinone, very close to that observed for the hydroquinone–quinone redox system. Also, a one-electron/one-proton process for the peak II, can be attributed to the oxidation of piperazinyl-imino moiety of the molecule [17–19].

Here, adsorption of RIF on the modified electrode surface can be used as an effective pre-concentration step prior to its voltammetric determination and it is necessary to select the variables affecting the adsorptive process. To avoid saturation of the electrode surface and to account for a reasonable response sensitivity and repeatability, an accumulation time of 260 s was used for the following experiments. In addition, it was found that the accumulation potential has no influence on the oxidation peak current. Accordingly, an open-circuit accumulation of RIF was performed in all investigations (Fig. S5).

3.2.2. *Analytical characteristics*

Under the optimized operating conditions, the anodic peak currents in LSVs were proportional to RIF concentration in the linear range of 0.006–10 μmol L^{-1} with regression eq. (1) and another linear range of 0.04–10 μmol L^{-1} with regression eq. (2), considering peak I and peak II as an analytical signal, respectively (Fig. 6).

$$I(\mu A) = 0.72C_{RIF}(\mu\text{mol L}^{-1}) + 0.14 \ (R^2 = 0.996) \quad (1)$$

$$I(\mu A) = 1.28C_{RIF}(\mu\text{mol L}^{-1}) + 0.12 \ (R^2 = 0.998) \quad (2)$$

The resulted detection limits for the determination of RIF using peaks I and II was 4.16 nmol L^{-1} and 2.34 nmol L^{-1} (based on S/N=3), respectively. Table 1 compares the response characteristics of the $Ni(OH)_2$–RGO/GCE with those of other modified electrodes reported in the literature for the determination of RIF.

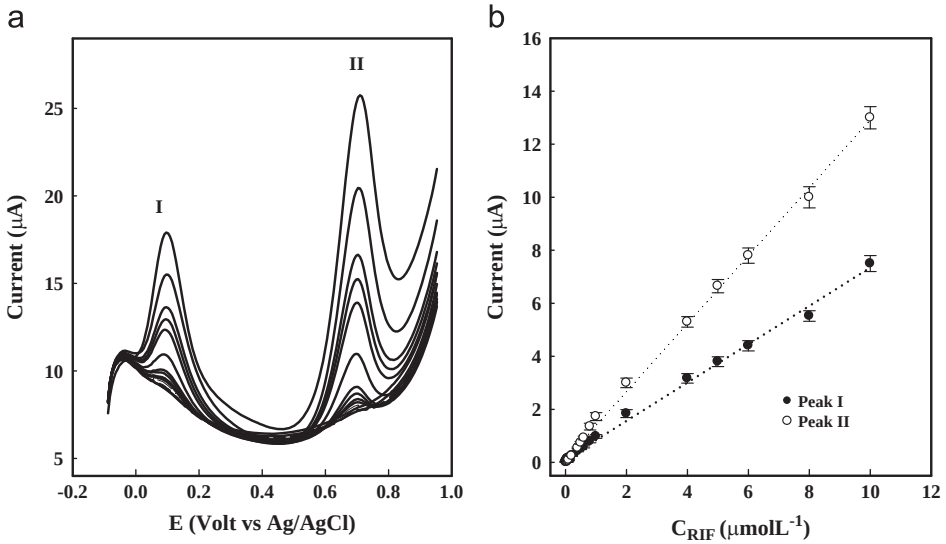

Fig. 6. (a) LSVs for various concentrations of RIF in the range of 0.006–10 μmol L^{-1}, supporting electrolyte was 0.1 mol L^{-1} PBR solution (pH 7.0). (b) Corresponding linear calibration curve of peak (I) and (II) currents vs. RIF concentration.

Table 1
Comparison of different modified electrodes for determination of RIF.

Electrode	Method	Linear range (μmol L^{-1})	Sensitivity (μA/μmol L^{-1})	LOD (nmol L^{-1})	Reference
CPE[a]	SWAdASV[b]	0.1–6	0.741	50	12
HMDE[c]	DPAdSV[d]	0.033–0.38	0.712×10^{-5}	6.13	26
ß-CD-PPY-Pt[e]	Chronoamprometry	2.61–25.23	0.00252	1690	28
HMDE	DPP[f]	0.1–10	0.0095	10	30
$Ni(OH)_2$–RGO–GCE	LSV	0.004–10	1.28	2.34	This work

[a] Carbon paste electrode.
[b] Square-wave adsorptive anodic stripping voltammetry.
[c] Hanging mercury dropping electrode.
[d] Differential pulse adsorptive stripping voltammetry.
[e] ß-cyclodextrin-polypyrrol platinum electrode.
[f] Differential pulse polarography.

As can be seen in this table, the present method exhibits more appropriate analytical characteristics including, low detection limit, high sensitivity and wide linear dynamic ranges for the electrochemical determination of RIF. The reproducibility for determination of 10 μmol L^{-1} RIF was evaluated by five independently prepared modified electrodes and the resulted RSD was 3.5% ($n=3$). The RSD of the peak currents of 10 μmol L^{-1} RIF for five repeated determinations with the same $Ni(OH)_2$–RGO/GCE was also 2.8%. In this work, any adsorbed RIF or its oxidation product was counteracted by applying ten CVs in supporting electrolyte (0.1 mol L^{-1} PBS of pH 7.0) between measurements, thereby obviating the fouling problems and renewing the electrode surface. Thus, the results herein indicate that the modified electrode has an excellent repeatability in both preparation and determination steps. Additionally, the interference effects of dopamine (DP), uric acid (UA), ascorbic acid (AA) and glucose (Glu) were tested on the voltammetric response of 10 μmol L^{-1} RIF (Fig. 7). No change in the response current of RIF was observed in the presence of these compounds or mixtures in them. Therefore, this method can be successfully applied for the simultaneous determination of RIF in the presence of the other interference compounds in the clinical preparations.

3.2.3. Analytical application to real matrices

The reliability of the modified electrode for drug analysis was assessed for determination of RIF tablet using a standard addition recovery method. The results showed that tablet matrix does not have any interference effect on the electrochemical analysis of RIF. The resulted amount for RIF content was 315.33 mg per tablet with RSD of 3.1% ($n=3$), indicating adequate precision and accuracy of the proposed electrode (Fig. S6).

Besides, the recovery studies of the spiked RIF in a human blood serum sample showed average value of 100.4% (Table 2), suggesting the successive applicability of the proposed strategy for the clinical applications.

4. Conclusions

In summary, electrochemically deposition has been used as a green, fast and simple approach for preparation of nickel hydroxide–reduced graphene oxide thin film as a highly reproducible and stable modifier on the surface of glassy carbon electrode.The excellent conductivity, the large surface area, and the remaining oxygen-related defects of the RGO film make it a convenient substrate for deposition of nickel hydroxide nanoparticles. Then, we characterized the $Ni(OH)_2$NPs–RGO nano-film both qualitatively and quantitatively, providing a simple and novel method for the development of voltammetric sensors. Excellent sensory characteristics provide the successful application of this sensor for the accurate determination of trace amounts of RIF in pharmaceutical and clinical preparations. Thus, it is believed that this new

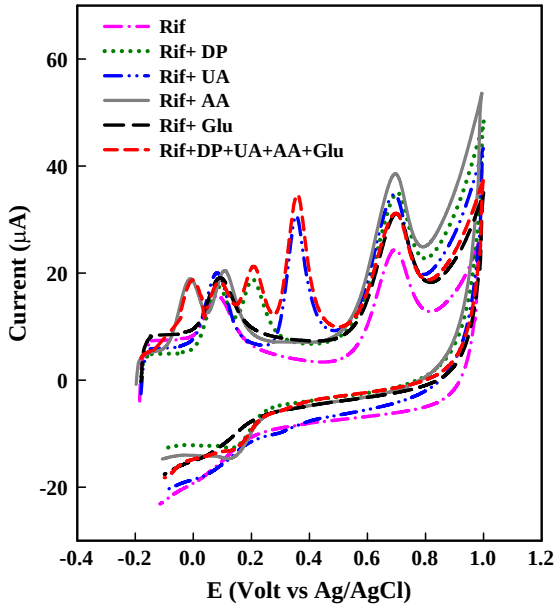

Fig. 7. CVs of $Ni(OH)_2$–RGO/GCE for the determination of 10 μmol L^{-1} Rifampicin (dashed-dotted line, pink) and 10 μmol L^{-1} rifampicin in the presence of 10 μmol L^{-1} DP (dotted line, green), 1 mmol L^{-1} UA (dashed-dotted-dotted line, blue), 10 μmol L^{-1} AA (solid line, gray), 1 mmol L^{-1} Glu (medium dashed line, black) and the mixture of DP, UA, AA and Glucose interferences (short dashed line, red) in 0.1 mol L^{-1} phosphate buffer solution (pH 7.0). Scan rate: 100 mV s^{-1}. (For interpretation of the references to color in this figure legend, the reader is referred to the web version of this article.)

Table 2
Recovery results of RIF analysis spiked in plasma samples[a].

No.	Spiked (μmol L^{-1})	Found (μmol L^{-1})	Recovery (%)
1	0.01	0.0096 ± 0.001	96
2	0.06	0.0620 ± 0.011	103.33
3	0.1	0.0983 ± 0.015	98.30
4	2	1.9740 ± 0.140	98.70
5	6	6.3410 ± 0.354	105.66

[a]Mean ± standard deviation ($n=3$) (rounded).

nano-layers can act as a novel platform for the next generation of electrochemical biosensors.

Acknowledgments

The authors gratefully acknowledge the support of this work by the Research Council and the Center of Excellence for Nanostructures of the Sharif University of Technology, Tehran, Iran. We are also thankful to Prof H.H. Girault's group (EPFL university-Switzerland) and Exir Daru pharmaceutical company (Tehran, Iran), respectively for kindly getting us the graphene oxide powder and rifampicin drug.

Appendix A. Supporting information

Supplementary data associated with this article can be found in the online version at http://dx.doi.org/10.1016/j.talanta.2013.10.047.

References

[1] C.I.L. Justino, T.A.P. Rocha-Santos, S. Cardoso, A.C. Duarte, Trends Anal. Chem. 47 (2013) 27–36.
[2] A.K. Geim, K.S. Novoselov, Nat. Mater. 6 (2007) 183–191.
[3] A.K. Geim, Science 324 (2009) 1530–1534.
[4] M.D. Stoller, S. Park, Y. Zhu, J. An, R.S. Ruoff, Nano Lett. 8 (2008) 3498–3502.
[5] M.J. McAllister, J.L. Li, D.H. Adamson, H.C. Schniepp, A.A. Abdala, J. Liu, M. H. Alonso, D.L. Milius, R. Car, R.K. Prud'homme, I.A. Aksay, Chem. Mater. 19 (2007) 4396–4404.
[6] M.J. Allen, V.C. Tung, R.B. Kaner, Chem. Rev. 110 (2010) 132–145.
[7] F. Yavari, N. Koratkar, J. Phys. Chem. Lett. 3 (2012) 1746–1753.
[8] S. Kochmann, T. Hirsch, O.S. Wolfbeis, Trends Anal.Chem. 39 (2012) 87–113.
[9] Y. Liu, X. Dong, P. Chen, Chem. Soc. Rev. 41 (2012) 2283–2307.
[10] D. Chen, H. Feng, J. Li, Chem. Rev. 12 (2012) 6027–6053.
[11] K.R. Ratinac, W. Yang, J.J. Gooding, P. Thordarson, F. Braet, Electroanalysis 23 (2011) 803–826.
[12] M. Pumera, Chem. Rec. 9 (2009) 211–223.
[13] Y. Shao, J. Wang, H. Wu, J. Liu, I.A. Aksay, Y. Lin, Electroanalysis 22 (2010) 1027–1036.
[14] J. Yang, S. Deng, J. Lei, H. Ju, S. Gunasekaran, Biosens. Bioelectron. 29 (2011) 159–166.
[15] Y. Zhou, J.J. Chen, F.B. Wang, Z.H. Sheng, X.H. Xia, Chem. Commun. 46 (2010) 5951–5953.
[16] S. Wu, Z. Yin, Q. He, G. Lu, Q. Yan, H.J. Zhang, Phys. Chem. C 115 (2011) 15973–15979.
[17] F.S. Gutierrez, C.M.J. Lobo, O.A.J. Miranda, B.P. Tunon, G.A. Carriedo, A.F.J. Garca, J.I. Fidalgo, Electroanalysis 13 (2001) 1399–1404.
[18] F.S. Gutierrez, L.M.C. Blanco, C.M.J. Lobo, O.A.J. Miranda, B.P. Tunon, Electroanalysis 16 (2004) 1660–1666.
[19] E. Hammam, A.M. Beltagi, M.M. Ghoneim, Microchem. J. 77 (2004) 53–62.
[20] A. Srivastava, D. Waterhouse, A. Ardrey, S.A. Ward, J.Pharmaceut. Biomed. Anal. 70 (2012) 523–528.
[21] P.F. Fang, H.L. Cai, H.D. Li, R.H. Zhu, Q.Y. Tan, W. Gao, P. Xu, Y.P. Liu, W.Y. Zhang, Y.C. Chen, F. Zhang, J. Chromatogr. B 878 (2010) 2286–2291.
[22] I. Ganescu, G. Bratulescu, B. Lilea, A. Ganescu, A. Barbu, Acta Chim. Slov 49 (2002) 339–345.
[23] M.A.A. Lomillo, O.D. Renedo, M.J.A. Martınez, Electroanalysis 14 (2002) 634–637.
[24] M.A.A. Lomillo, J.M. Kauffmann, M.J.A. Martinez, Biosens. Bioelectron. 18 (2003) 1165–1171.
[25] M.A.A. Lomillo, O.D. Renedo, M.J.A. Martinez, Electrochim. Acta 50 (2005) 1807–1811.
[26] R.H.T. Santos, N.G. Santos, J.P.H. Alves, C.A.B. Garcia, L.C.P. Romao, M.L.P. M. Arguelho, Bioelectrochem 72 (2008) 122–126.
[27] Y. Hahn, S. Shin, Arch. Pharm. Res. 24 (2001) 100–104.
[28] E. Sharifi, A. Salimi, E. Shams, Biosens.Bioelectron. 45 (2013) 260–266.
[29] L.A. Hutton, M. Vidotti, A.N. Patel, M.E. Newton, P.R. Unwin, J.V.J. Macpherson, Phys. Chem. C 115 (2011) 1649–1658.
[30] C. Natarajan, H. Matsumoto, G. Nogami, J. Electrochem. Soc. 144 (1997) 121–126.
[31] K.E. Toghill, L. Xiao, N.R. Stradiotto, R.G. Compton, Electroanalysis 22 (2010) 491–500.
[32] K.E. Toghill, L. Xiao, M.A. Phillips, R.G. Compton, Sens.Actuators B 147 (2010) 642–652.
[33] L.L. Zhang, X. Zhao, M.D. Stoller, Y. Zhu, H. Ji, S. Murali, Y. Wu, S. Perales, B. Clevenger, R.S. Ruoff, Nano Lett. 12 (2012) 1806–1812.
[34] H.L. Guo, X.F. Wang, Q.Y. Qian, F.B. Wang, X.H. Xia, ACS Nano 3 (2009) 2653–2659.
[35] Y.Y. Shao, J. Wang, M. Engelhard, C.M. Wang, Y.M. Lin, J. Mater. Chem. 20 (2010) 743–748.
[36] M. Zhou, Y.L. Wang, Y.M. Zhai, J.F. Zhai, W. Ren, F. Wang, S. Dong, J. Chem. Eur. J. 15 (2009) 6116–6120.
[37] S. William, J.R. Hummers, E.O. Richard, J. Am. Chem. Soc. 80 (1958) 1339. (1339).
[38] Y. Zhou, G. Zhang, J. Chen, G.E. Yuan, L. Xu, L. Liu, F. Yang, Electrochem. Commun. 22 (2012) 69–72.
[39] E. Laviron, J. Electroanal. Chem. 52 (1974) 355–365.
[40] R.S. Nicholson, I. Shain, Anal. Chem. 36 (1964) 706–723.
[41] I. Streeter, G.G. Wildgoose, L. Shao, R.G. Compton, Sens. Actuators B 133 (2008) 462–466.
[42] L. Xiao, L. Wi, G.G. Wildgoose, R.G. Compton, Sens. Actuators B 138 (2009) 524–538.
[43] E. Laviron, J. Electroanal. Chem. 101 (1979) 19–28.